IOP Publishing Physica Scripta
Phys. Scr. **95** (2020) 035502 (9pp) https://doi.org/10.1088/1402-4896/ab52d1

Dynamics of chirped finite Olver Gaussian beam propagating paraxial to uniaxial crystal

Long Jin

Department of Basic Science, Hubei University of Automotive Technology, 167 Checheng West Road, Shiyan City 442002, Hubei province, People's Republic of China

E-mail: crazyjinlong@163.com and 20140007@huat.edu.cn

Received 7 August 2019, revised 19 October 2019
Accepted for publication 30 October 2019
Published 28 January 2020

Abstract

Paraxial transmission characteristic of a second-order frequency chirped finite Olver Gaussian beam (CFOGB) in the uniaxial crystal orthogonal to the optical axial is investigated based on the generalized Huygens–Fresnel integral equation. The exact expression for the CFOGB passing through the uniaxial crystal is derived. The contour graph of the CFOGB intensity distribution on some transversal cross sections, the side view of this beam propagating in three different kinds of uniaxial crystal models are discussed, the influence of the frequency chirp parameter on the beam evolution properties is explored as well. We make sure that the formulae and the conclusions obtained can provide an effective and quick method to adjust and control this CFOGB evolution path and profile through choosing the proper uniaxial crystal structure and frequency chirp value to meet the practical usage.

Keywords: laser beam characterization, chirped finite Olver gaussian beam, uniaxial crystal, generalized huygens-fresnel integral equation

(Some figures may appear in colour only in the online journal)

1. Introduction

As a novel type of realizable beam, the finite Airy beam (FAiB) was first theoretical and experimental introduced by Siviloglou *et al* in 2007 [1, 2]. This wave exhibits three kinds of outstanding properties of self-acceleration, self-healing and non-diffracting during the propagation in the different varieties of media [3–5], which have been widely examined and verified in the past few years. Just like Bessel beam is made up various kinds of orders, the finite Olver beam (FOB) family was proposed recently by Belafhal and his collaborators as the solution of the Olver's differential equation [6]. The zeroth-order FOB was presented theoretically and numerically as the well-known FAiB in their work, meanwhile, the generation's masks of the FOB in the zeroth and first orders are given based on a computer generated holograms method in that paper as well. To date, the FOB and finite Olver Gaussian beam (FOGB) propagating in a paraxial *ABCD* optical system [7], a medium of basis annular aperture [8], an apertured misaligned *ABCD* optical system [9] and double negative index slab system [10] have been intensely discussed within the context of laser optics, besides these, Besieris *et al* newly gave a note on self-accelerating Olver and Olver–Gauss beams [11]. For another, the frequency chirp is a phenomenon existing in wide scopes of an ultrashort intense laser pulse, where the signal frequency varies over time [12]. The exploration of frequency chirped pulse in *ABCD* optical system or dispersion medium has practical significance in optical communication, because the wave spectrum is influenced and widened when this frequency chirp is imposed externally on the incident beam. As far as we know, the evolution properties of the FAiB and Airy derivative beams with frequency chirp term in optical slab waveguide contained double negative material and right handed material and optical fiber were checked [13–15] in half a dozen years ever since the first experimental realization of controlling the chirped laser pulse by Melinger *et al* [16]. In the year of 2019, Jin goes a step further to probe the transformation of frequency chirped two-dimensional FOGB through sandwich structured slab [17].

Uniaxial crystal like rutile displays important role in optical communication devices design due to the polarization state of the travelling wave goes through a conversion, many anisotropic media, for instance, polarizer, photonic fiber,

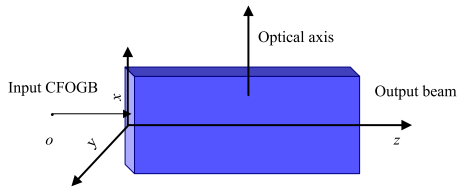

Figure 1. Geometry of the input CFOGB propagating in auniaxial crystal.

switch, compensator, and etc were commercialized and employed in a lot of experiments situation [18, 19]. Ciattoni and Palma perform for the first time the propagation of wave evoluting in the uniaxial crystal orthogonal to the optical axial by solving the boundary value of the ordinary and extraordinary beams, respectively, which avoids the sophisticated mathematical computation in dealing with Maxwell's equations [20]. So far, the propagation of the FAiB in the anisotropic uniaxial crystal under the paraxial approximation and beyond have been studied by Deng *et al* [21, 22], the non-paraxial propagation of the chirped Airy vortex beam, Airy–Gaussian vortex beam and the radially polarized Airy–Gaussian beams with different initial launch angles in uniaxial crystals were also explored by her research group [23–25]. What is more, the transformation characteristics of the FOGB through a uniaxial crystal was examined by Hennani *et al* [26], however, the input beam distribution presented in reference [26] appears to be Gaussian profile and cannot be used to delineate the FOGB properties entirely, therefore, they merely finished the propagation of the FOB, without Gaussian term, cutting through the uniaxial crystal orthogonal to the optical axial. All in all, last time we checked, there is no literature exploring the evolution of frequency chirped finite Olver Gaussian beam (CFOGB) in the uniaxial crystal orthogonal to the optical axial.

Therefore, in the rest of this letter, we systematically explore the second-order CFOGB intensity profiles on several transversal cross sections, and the side view of this beam propagating in the uniaxial crystal. The remainder of the paper is organized as follows: firstly, in section 2, the analytical expression of the CFOGB passing through the paraxial uniaxial crystal is calculated in space domain by using the generalized Huygens–Fresnel integral equation. In section 3, the contour graph and side view of the FOGB propagating in three kinds of uniaxial crystal are thoroughly studied, respectively; meanwhile, the influence of the frequency chirp parameter on the CFOGB intensity distribution is analyzed as well. Finally, a simple conclusion is summarized at the end of section 4.

2. Physical model and analytical expression

The schematic diagram of a laser beamlet cutting through the uniaxial crystal orthogonal to the optical axis is described in figure 1. We assume that the uniaxial crystal is lossless with its optical axis being the x-axis, y-axis being another transversal direction, and the observation plane is set as the xy-plane in the Cartesian coordinate system, whereas the z-axis is taken to be the propagation axis. Considering that the CFOGB is linearly in x-axis and is incident on the uniaxial crystal, its electric field distribution at input plane $z = 0$ (point O) can be written as [17]

$$E_x(x_0, y_0, z = 0) = O_m\left(\frac{x_0}{\mu\omega_0}\right)\exp\left(a_0\frac{x_0}{\mu\omega_0}\right) \times O_n\left(\frac{y_0}{\mu\omega_0}\right)\exp\left(a_0\frac{y_0}{\omega_0}\right) \times \exp\left(-\mathrm{i}C_0\frac{x_0^2 + y_0^2}{\omega_0^2}\right), \quad (1)$$

and

$$E_y(x_0, y_0, z = 0) = 0, \quad (2)$$

where ω_0 is the beam waist length of the incident beam, μ is named as the corresponding adjustment factor regulating the beam spot size, a_0 denotes the truncation parameter, by means of which the pseudo non-diffracting Olver beam carries finite energy, and C_0 characters the frequency chirp coefficient. The kernel O denotes the Olver function with the subscript m (or n) being the function order, and has been defined as

$$O_n(x_1) = \frac{1}{2\pi} \times \int_{-\infty}^{+\infty} \exp\left[a(\mathrm{i}u)^\gamma + \mathrm{i}ux_1\right]\mathrm{d}u, \quad (3)$$

with

$$\begin{cases} \gamma = n + 3 \\ |a| = \dfrac{1}{n+3} \end{cases}. \quad (4)$$

One can easily recognize from equation (3) that the traditional Airy function feature is acted out as long as the Olver function order $n = 0$. In the frame of this reference, the relative dielectric tensor of the uniaxial crystal is taken the form as [27]

$$\varepsilon = \begin{pmatrix} n_e^2 & 0 & 0 \\ 0 & n_o^2 & 0 \\ 0 & 0 & n_o^2 \end{pmatrix}, \quad (5)$$

where n_o and n_e are the traditional ordinary and extraordinary refractive index of this crystal, respectively. Here, we define a notation $t = n_e/n_o$, which is termed as the ratio of the extraordinary refractive index to the ordinary refractive index. There are three kinds of uniaxial crystal, generally, the positive, the negative and the isotropy one, of which the t is greater than 1, less than 1 and equal to 1, respectively.

Under the paraxial approximation, the two electric field components of the CFOGB propagating in the uniaxial crystal can be evaluated by the following generalized Huygens–Fresnel integral theory, which can be deduced by using the angular spectrum method, for more information, please refer to the literature [20, 28, 29]

$$E_x(x, y, z) = \left(\frac{\mathrm{i}kn_o}{2\pi z}\right)\mathrm{e}^{-\mathrm{i}kn_e z}\iint_{s_1} E_x(x_0, y_0, 0) \times \mathrm{e}^{\left(-\frac{\mathrm{i}k}{2zn_e}[n_o^2(x-x_0)^2 + n_e^2(y-y_0)^2]\right)}\mathrm{d}x_0\mathrm{d}y_0, \quad (6)$$

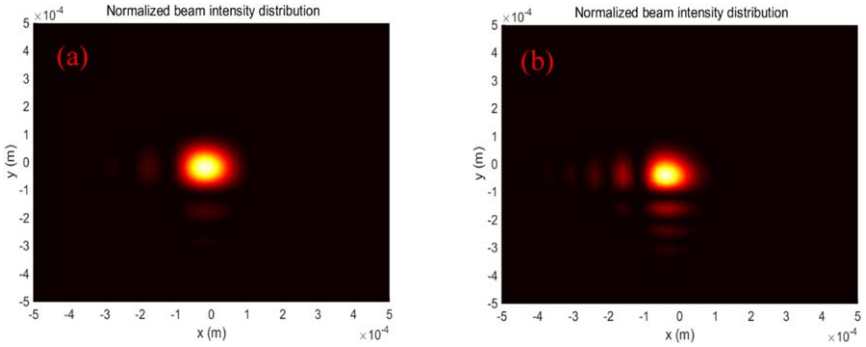

Figure 2. Incident FOGB intensity distribution with two kinds of beam order n, $\lambda = 1.55$ μm, $a_0 = 0.2$, $\omega_0 = 1$ mm, $\mu = 0.05$ and $C_0 = 0$; (a) $n = 2$; (b) $n = 0$.

$$E_y(x, y, z) = \left(\frac{\mathrm{i}kn_o}{2\pi z}\right)\mathrm{e}^{-\mathrm{i}kn_o z}\int\int_{s_1} E_y(x_0, y_0, 0) \times \mathrm{e}^{\left(-\frac{\mathrm{i}kn_o}{2z}[(x-x_0)^2+(y-y_0)^2]\right)}\mathrm{d}x_0\mathrm{d}y_0, \tag{7}$$

where $k = 2\pi/\lambda$ is the wave number, with λ being the input wave length. It is easily obtained that the equation (7) exhibits a standard Fresnel behavior, but the extraordinary expression (6) reveals the anisotropic dynamics. Inserting equations (1) and (2) into equations (6) and (7), separately, one obtains the closed-form complex electric field of the CFOGB after passes through the uniaxial crystal as

$$E_x(x, y, z) = \frac{\mathrm{i}kn_o}{2z}\sqrt{\frac{1}{M_1 M_2}}\exp(-\mathrm{i}kn_e z) \times \exp\left(\frac{-\mathrm{i}k(n_o^2x^2 + n_e^2y^2)}{2zn_e}\right)U(x, z)U(y, z), \tag{8}$$

where

$$U(x, z) = \exp\left(-\frac{k^2n_o^4x^2}{4M_1z^2n_e^2} + \frac{a_0^2}{4M_1\mu^2\omega_0^2} + \frac{\mathrm{i}ka_0xn_o^2}{2M_1z\mu\omega_0n_e} + \frac{1}{96M_1^3\mu^6\omega_0^6} + \frac{\mathrm{i}kxn_o^2}{8M_1^2\mu^3\omega_0^3zn_e} + \frac{a_0}{8M_1^2\mu^4\omega_0^4}\right) \times O_m\left(\frac{\mathrm{i}kxn_o^2}{2M_1z\mu\omega_0n_e} + \frac{a_0}{2M_1\mu^2\omega_0^2} + \frac{1}{16M_1^2\mu^4\omega_0^4}\right), \tag{9}$$

$$U(y, z) = \exp\left(-\frac{k^2n_e^4y^2}{4M_2z^2} + \frac{a_0^2}{4M_2\mu^2\omega_0^2} + \frac{\mathrm{i}ka_0yn_e}{2M_2z\mu\omega_0} + \frac{1}{96M_2^3\mu^6\omega_0^6} + \frac{\mathrm{i}kyn_e}{8M_2^2\mu^3\omega_0^3z} + \frac{a_0}{8M_2^2\mu^4\omega_0^4}\right) \times O_n\left(\frac{\mathrm{i}kyn_e}{2M_2z\mu\omega_0} + \frac{a_0}{2M_2\mu^2\omega_0^2} + \frac{1}{16M_2^2\mu^4\omega_0^4}\right), \tag{10}$$

with

$$M_1 = \frac{\mathrm{i}C_0}{\omega_0^2} + \frac{\mathrm{i}kn_o^2}{2zn_e}, \tag{11}$$

$$M_2 = \frac{\mathrm{i}C_0}{\omega_0^2} + \frac{\mathrm{i}kn_e}{2z}, \tag{12}$$

and

$$E_y(x, y, z) = 0. \tag{13}$$

Finally, the light intensity of the output CFOGB is gained with ease by using the complex conjugate of $E_x(x, y, z)$

$$I = \frac{n_0}{2c\mu_0}|E_x(x, y, z)|^2 \propto |E_x(x, y, z)|^2, \tag{14}$$

where the proportional constant is connected with the refractive index n_0 of the beam transmitting in free space, the speed of light c and the permeability μ_0 in vacuum.

3. Results and analysis

3.1. Incident FOGB profile with different beam order

We begin our analysis by discussing the incident FOGB intensity contour graph with two different beam order n, the result is depicted in figure 2, and some specific parameters are set as $\lambda = 1.55$ μm, $a_0 = 0.2$, $\omega_0 = 1$ mm, $\mu = 0.05$ and $C_0 = 0$ without chirp stimulated. One can clearly see that the lateral petals rapidly decrease with the increasing of beam order n, and there are only a very small amount of lateral petals when the input FOGB $n = 2$, but the profile outlines of these two kinds of incident beams are more or less the same compared with figures 2(a) and (b).

3.2. Each order FOGB evolution characteristics changed with the factor t

In the next moment, we focus on the contour graph of the second-order FOGB intensity distribution on several transmission cross sections changed with the ratio of the extraordinary refractive index to the ordinary refractive index t while this beam transmits in the uniaxial crystal, the simulation result is demonstrated in figure 3, here we choose the parameters as $n_o = 1.5$ fixed, the Rayleigh length of the input beam is $Z_R = \pi\mu^2\omega_0^2/\lambda = 0.0051$ m, and other factors are

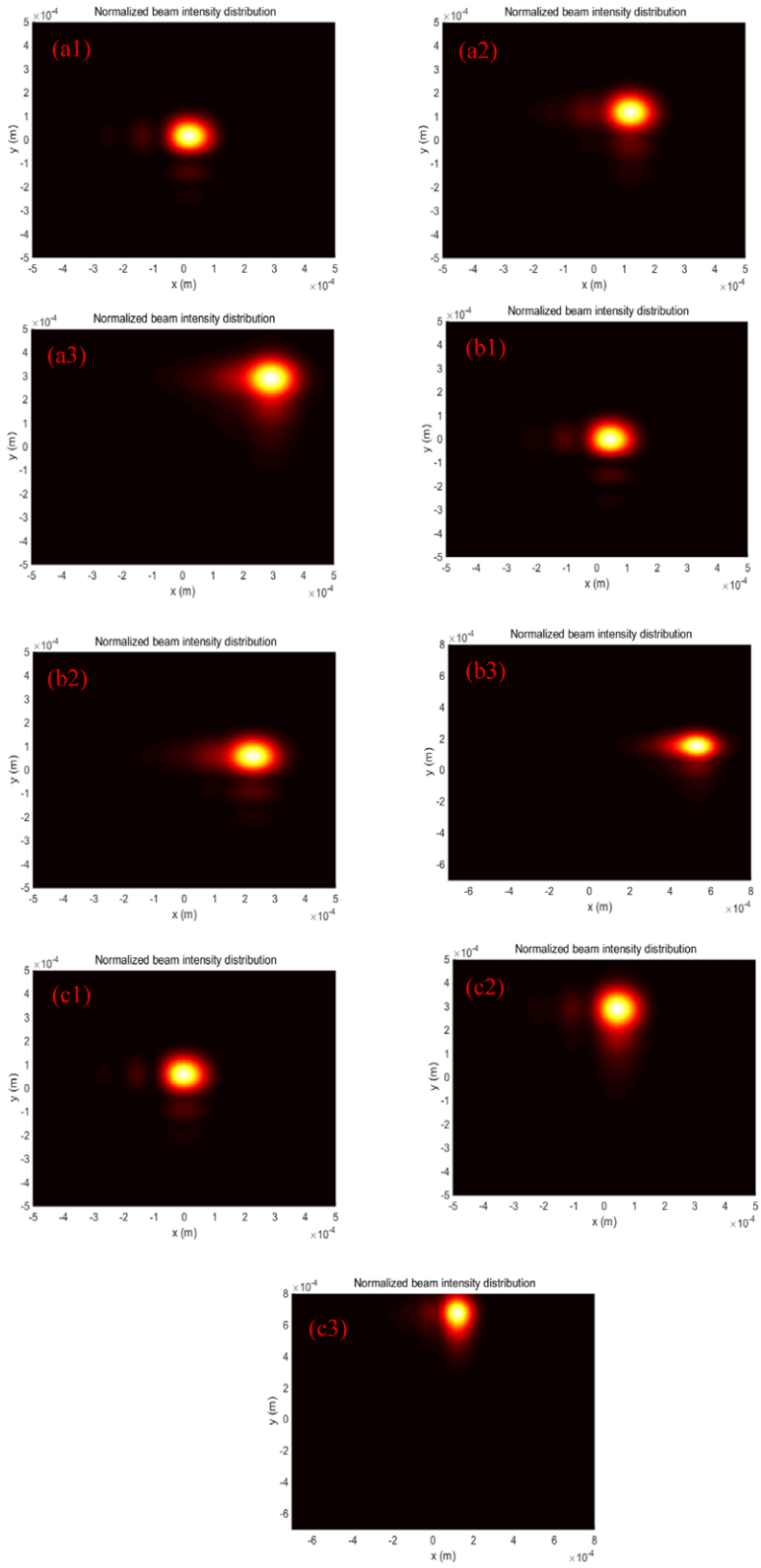

Figure 3. Contour graph of the second-order FOGB intensity distribution on several transmission cross sections of the uniaxial crystal changed with the ratio of the extraordinary refractive index to the ordinary refractive index t, $n = 2$, $\lambda = 1.55$ μm, $a_0 = 0.2$, $\omega_0 = 1$ mm, $\mu = 0.05$, $C_0 = 0$, $Z_R = \pi\mu^2\omega_0^2/\lambda = 0.0051$ m and $n_o = 1.5$ fixed; (a1) $n_e = 1.5$, $t = 1$, $z = 5Z_R$, (a2) $n_e = 1.5$, $t = 1$, $z = 10Z_R$, (a3) $n_e = 1.5$, $t = 1$, $z = 15Z_R$; (b1) $n_e = 2.0$, $t = 1.33$, $z = 5Z_R$, (b2) $n_e = 2.0$, $t = 1.33$, $z = 10Z_R$, (b3) $n_e = 2.0$, $t = 1.33$, $z = 15Z_R$; (c1) $n_e = 1.0$, $t = 0.67$, $z = 5Z_R$, (c2) $n_e = 1.0$, $t = 0.67$, $z = 10Z_R$, (c3) $n_e = 1.0$, $t = 0.67$, $z = 15Z_R$.

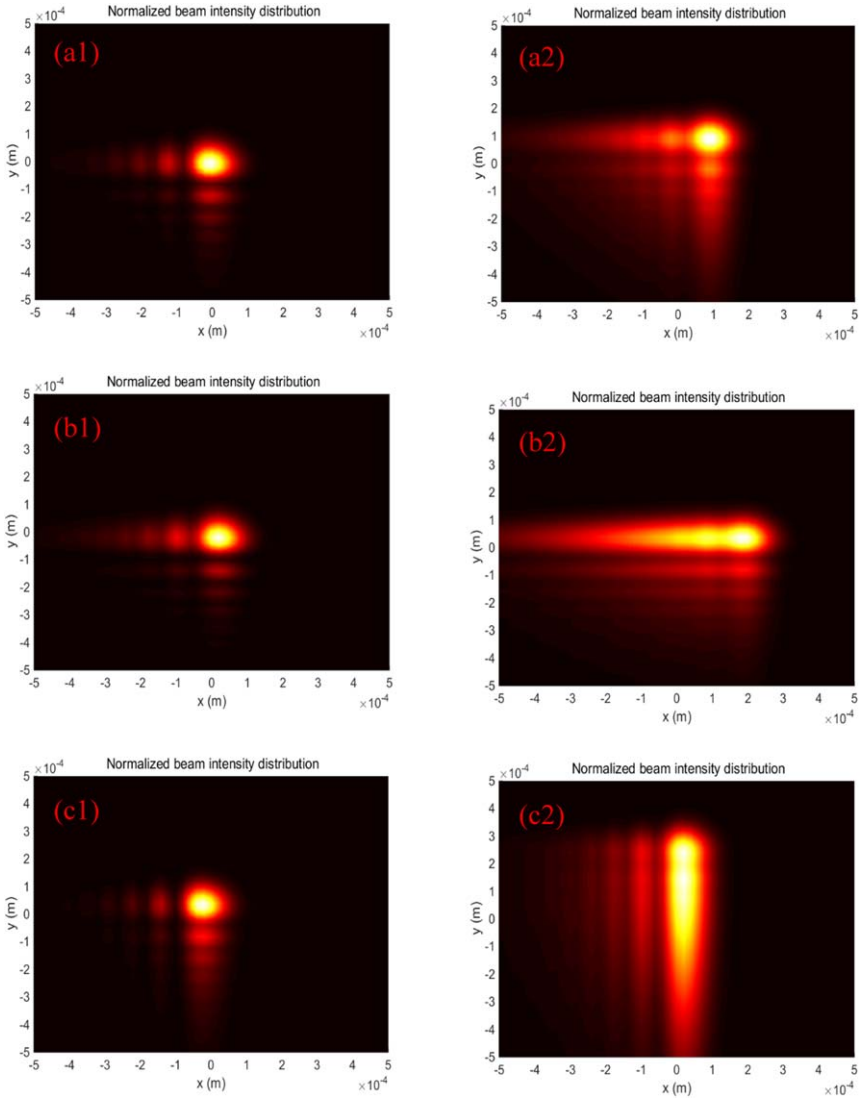

Figure 4. Contour graph of the zeoth-order FOGB intensity distribution on several transmission cross sections of the uniaxial crystal changed with the ratio of the extraordinary refractive index to the ordinary refractive index t, $n = 0$, $\lambda = 1.55$ μm, $a_0 = 0.2$, $\omega_0 = 1$ mm, $\mu = 0.05$, $C_0 = 0$, $Z_R = \pi\mu^2\omega_0^2/\lambda = 0.0051$ m and $n_o = 1.5$ fixed; (a1) $n_e = 1.5$, $t = 1$, $z = 5Z_R$, (a2) $n_e = 1.5$, $t = 1$, $z = 10Z_R$; (b1) $n_e = 2.0$, $t = 1.33$, $z = 5Z_R$, (b2) $n_e = 2.0$, $t = 1.33$, $z = 10Z_R$; (c1) $n_e = 1.0$, $t = 0.67$, $z = 5Z_R$, (c2) $n_e = 1.0$, $t = 0.67$, $z = 10Z_R$.

completely the same as those in figure 2. By viewing these figures, it is recognized that the second-order FOGB, too, has the ability of self-bending, i.e. this beam curves along the parabola with the increasing of transmission distance. When $n_o = n_e = 1.5$ ($t = 1$) in isotropic medium in figure 3(a), the beam accelerates along the $\pi/4$ axis in any transversal plane, manifesting that the bends degree in two transversal directions are always the same along with the increased distance. Upon evolution in the positive uniaxial crystal ($n_e = 2.0$, $t = 1.33$) in figure 3(b2), the self-bends of the FOGB in the y-direction (i.e. the transversal direction orthogonal to the optical axis) are slower than that in the x-direction due to the anisotropic effect of the crystal, and the central bright point moves to the ($x = 0.53\omega_0$, $y = 0.17\omega_0$) when $z = 15Z_R$ in figure 3(b3). However, if the uniaxial crystal is negative ($n_e = 1.0$, $t = 0.67$), the acceleration of the beam in y-direction is much faster than that in optical axis x-direction, as shown in figures 3(c2) and (c3). What is more, it is worthy to mention that the contour plots of the second-order FOGB intensity distribution for three different kinds of uniaxial crystals are approximately the same in near range (e.g. $z \leqslant 5Z_R$), regardless of the ratio of the extraordinary refractive index to the ordinary refractive index t, the reason is that the anisotropic effect of the crystal can be neglected while beam transmits in a very short propagation distance z. The zeroth-order FOGB intensity outline on different intersecting surface of the uniaxial crystal for several values of t is also depicted in figure 4. One can distinctly recognize from these figures that the acceleration dynamics for two kinds of beams are the same in the uniaxial crystal when the values of t are equal. In addition, because there are much more lateral petals, the influence of the anisotropic effect on zeroth-order FOGB is more obvious than that of the second-order one, even in near range, as shown in figures 4(b1) and (c1). While propagating to the distance of $z = 10Z_R$, the interference of main lobe and side lobes is very serious in x-direction for the

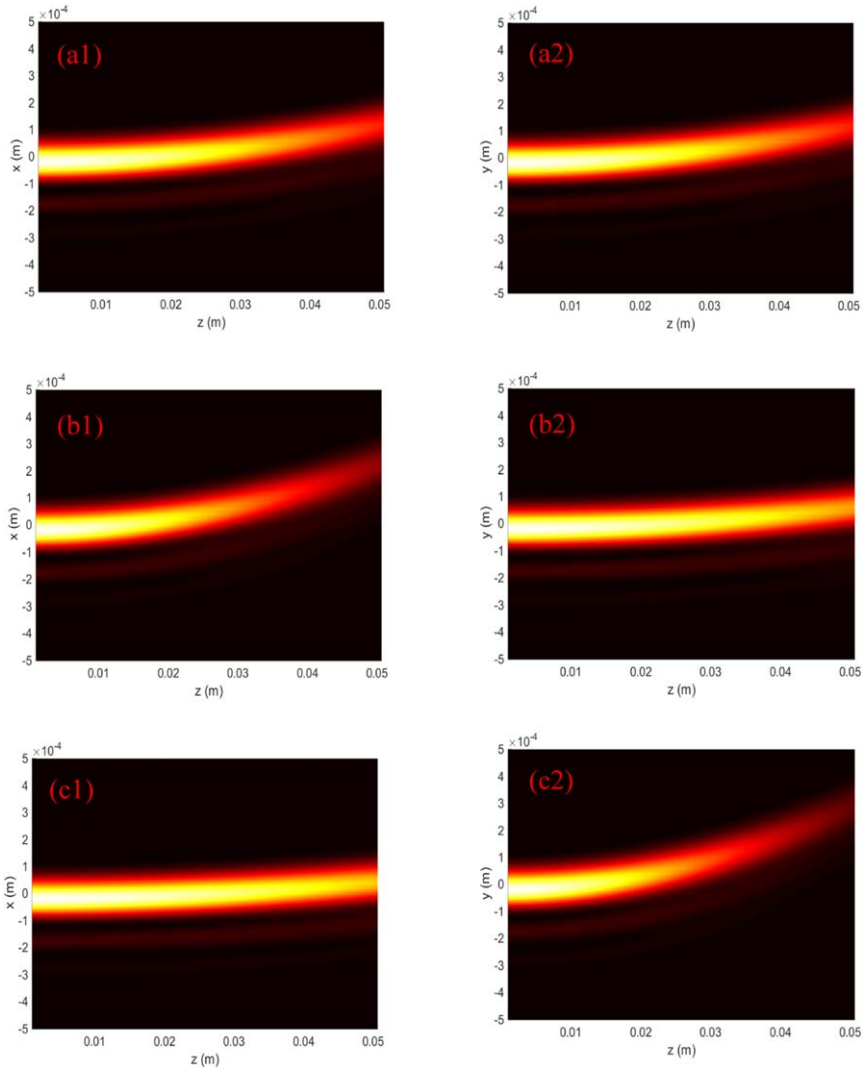

Figure 5. Side transmission view of the second-order FOGB intensity distribution while beam evoluting in the uniaxial crystal changed with the ratio of the extraordinary refractive index to the ordinary refractive index t, $n = 2$, $\lambda = 1.55$ μm, $a_0 = 0.2$, $\omega_0 = 1$ mm, $\mu = 0.05$, $C_0 = 0$, and $n_o = 1.5$ fixed; (a1) $n_e = 1.5$, $t = 1$, x-direction, (a2) $n_e = 1.5$, $t = 1$, y-direction; (b1) $n_e = 2.0$, $t = 1.33$, x-direction, (b2) $n_e = 2.0$, $t = 1.33$, y-direction; (c1) $n_e = 1.0$, $t = 0.67$, x-direction, (c2) $n_e = 1.0$, $t = 0.67$, y-direction.

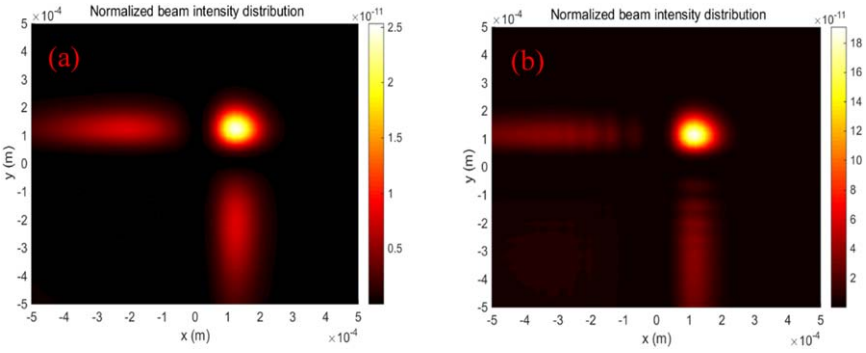

Figure 6. Contour graph of the FOGB intensity $|E_y(x, y, z)|^2$ on cross section $z = 10Z_R$ of the uniaxial crystal, $\lambda = 1.55$ μm, $a_0 = 0.2$, $\omega_0 = 1$ mm, $\mu = 0.05$, $C_0 = 0$, and $n_o = n_e = 1.5$ ($t = 1$); (a) $n = 2$; (b) $n = 0$.

positive uniaxial crystal, as shown in figure 4(b2), otherwise in figure 4(c2), the interference mainly appear in the y-direction.

The side transmission view of the second-order FOGB in x- and y-directions is explored in figure 5 in order to further illuminate the anisotropic effect of the uniaxial crystal. It is

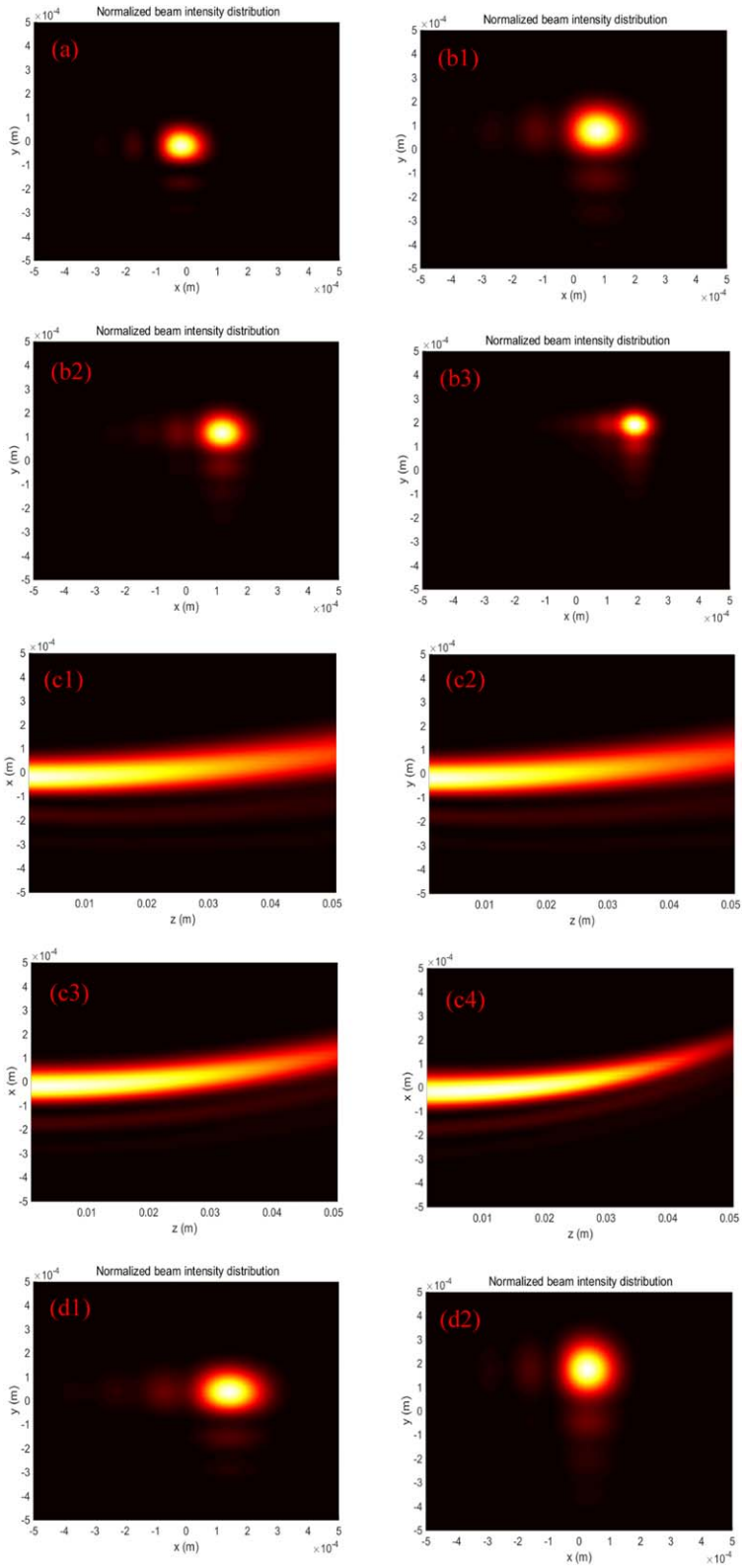

Figure 7. CFOGB and its intensity distribution when propagating in the uniaxial crystal, $n = 2$, $\lambda = 1.55$ μm, $a_0 = 0.2$, $\omega_0 = 1$ mm, $\mu = 0.05$, and $n_o = 1.5$ fixed; (a) incident beam profile; (b1) emerging beam profile, $n_e = 1.5$, $t = 1$, $C_0 = 20$; (b2) emerging beam profile, $n_e = 1.5$, $t = 1$, $C_0 = 0$; (b3) emerging beam profile, $n_e = 1.5$, $t = 1$, $C_0 = -20$; (c1) side view, $n_e = 1.5$, $t = 1$, $C_0 = 20$, x-direction; (c2) side view, $n_e = 1.5$, $t = 1$, $C_0 = 20$, y-direction; (c3) side view, $n_e = 1.5$, $t = 1$, $C_0 = 0$, x-direction; (c4) side view, $n_e = 1.5$, $t = 1$, $C_0 = -20$, x-direction; (d1) emerging beam profile, $n_e = 2.0$, $t = 1.33$, $C_0 = 20$; (d2) emerging beam profile, $n_e = 1.0$, $t = 0.67$, $C_0 = 20$.

evident that the acceleration of the FOGB speeds up in x-direction and slows down in y-direction while beam propagates in positive uniaxial crystal from figure 5(b), and the conclusion is the opposite when the uniaxial crystal is negative, as shown in figure 5(c), in other words, the symmetric of the beam intensity can only be achieved in the isotropic medium, as demonstrated in figure 5(a). Further analysis demonstrates that the bigger the t is under the event $t > 1$, or the smaller the t is if $t < 1$, the stronger the asymmetry of the beam outline is formed. These discussions verify the remark acquired in figure 3 once more.

In order to validate the paraxial theory of the FOGB propagating in the uniaxial crystal orthogonal to the optical axis, the non-paraxial beam intensity distribution $|E_y(x, y, z)|^2$ is portrayed in figure 6, here, we choose the maximum beam intensity in figure 3(a2) as the normalized factor, other parameters are in accord with those in figure 2 except $n_o = n_e = 1.5$ $(t = 1)$ and $z = 10Z_R$ fixed. It is explicitly seen from the colour bar of figures 6(a) and (b) that the intensity distribution of the y-component for both the second-order FOGB and zeroth-order one are extremely weaker compared with that of the x-component in figure 3(a2), manifesting that the paraxial approach is accurate enough when the beam waist size ω_0 is much larger than the wavelength λ.

3.3. Influence of frequency chirp on beam evolution properties

In this subsection, we are interested in the influence of the frequency chirp C_0 on the beam evolution, the numerical draw is demonstrated in figure 7. By comparing figure 7(a) with figure 2(a), we find that both the incident beam intensity profiles do not vary with chirp C_0, however, it is not the case for the second-order CFOGB propagating in the uniaxial crystal orthogonal to the optical axial. The emerging beam intensity distribution after passing through the whole crystal with three different values of C_0 is demonstrated in figure 7(b), by observing figures 7(b1)–(b3), it comes to the conclusion that the bigger the C_0 is, the larger the beam size, no matter the main lobe and the size lobes, is formed on the output plane, and vice versa. The CFOGB side views shown in figure 7(c) manifest that the acceleration property of the wave can be affected by the frequency chirp C_0 in both two transversal directions, when $C_0 = 20 > 0$ in figures 7(c1) and (c2), the self-bending of the CFOGB slows down to some extent than that of the $C_0 = 0$ (seen from figure 7(c3)), leading to the emerging beam profile close to the original point; on the contrary, the wave accelerates much faster while $C_0 = -20 < 0$, as shown in figure 7(c4). We also delineate the CFOGB profile evoluting in the anisotropic uniaxial crystals with different kinds of the ratio of the extraordinary refractive index to the ordinary refractive index t in figure 7(d), it is turned out that the emerging beam outline is a result of mutual effect of frequency chirp C_0 and factor t, therefore, we can adjust and control this CFOGB evolution path and profile through choosing the proper uniaxial crystal structure and chirp C_0 value to meet the practical use.

4. Conclusions

In summary, we have thoroughly investigated the evolution characteristics of the second-order CFOGB propagating in the uniaxial crystal orthogonal to the optical axial based on the generalized Huygens–Fresnel integral equation, the closed-form formulae for the CFOGB passing through the uniaxial crystal has been derived since it provides an effective method for analyzing the contour graph of the CFOGB intensity distribution on several transmission cross sections and the side view of this beam propagating in all kinds of uniaxial crystals, and avoids the sophisticated mathematical computation in dealing with Maxwell's equations. We found that the acceleration magnitude of the FOGB in the transversal direction orthogonal to the optical axis is typically different to that in the optical axis direction due to the anisotropic effect of the crystal, and the bigger the ratio of the extraordinary refractive index to the ordinary refractive index t is under the event $t > 1$, or the smaller the t is if $t < 1$, the stronger the asymmetry of the beam outline is formed. The influence of the frequency parameter C_0 on the beam evolution has been studied as well, it is concluded that C_0 plays an important role on the intensity profile evolution of the CFOGB when wave propagates in the uniaxial crystal that makes the beam outline, no matter the main lobe and the size lobes, towards the larger size when it is a bigger value, and vice versa, manifesting that the acceleration property of the wave can be affected by the frequency chirp C_0 in both two transversal directions, therefore, we can adjust and control this CFOGB evolution path and profile through choosing the proper uniaxial crystal structure and chirp C_0 value to meet the practical usage.

Acknowledgments

The authors gratefully acknowledge the financial support from the college innovation training program of Hubei University of automotive technology in China (No. DC 2018090, DC2018099).

References

[1] Siviloglou G A, Broky J, Dogariu A and Christodoulides D N 2007 *Phys. Rev. Lett.* **99** 213901
[2] Siviloglou G A and Christodoulides D N 2007 *Opt. Lett.* **32** 979–81
[3] Efremidis N K, Chen Z, Segev M and Christodoulides D N 2019 *Optica* **6** 1–17
[4] Zhou G, Chu X, Chen R and Zhou Y 2019 *Laser Phys.* **29** 025001
[5] Yue Y, Xiao H, Wang Z and Wu M 2013 *Acta Phys. Sin.* **62** 221–9
[6] Belafhal A, Ezzariy L, Hennani S and Nebdi H 2015 *Opt. Photonics J.* **5** 234–46
[7] Hennani S, Ezzariy L and Belafhal A 2015 *Opt. Photonics J.* **5** 273–94
[8] Hennani S, Ezzariy L and Belafhal A 2015 *Opt. Photonics J.* **5** 354–68
[9] Hennani S, Ezzariy L and Belafhal A 2017 *Optik* **136** 573–80

[10] Jin L and Zhang X 2018 *Chin. J. Phys.* **56** 1105–12
[11] Besieris1 I, Shaarawi A and Davis B 2019 *Opt. Photonics J.* **9** 1–7
[12] Dorsch R G, Lohmann A W, Bitran Y, Mendlovic D and Ozaktas H M 1994 *Appl. Opt.* **33** 7599–602
[13] Zhang L, Liu K, Zhong H, Zhang J, Li Y and Fan D 2015 *Opt. Express* **23** 2566–76
[14] Xie J, Zhang J, Ye J, Liu H, Liang Z, Long S, Zhou K and Deng D 2018 *Opt. Express* **26** 5845–56
[15] Zhong T, Zhang J, Feng L, Pang Z, Wang L and Deng D 2018 *J. Opt. Soc. Am.* B **35** 1354–61
[16] Melinger J S, Gandhi S R, Hariharan A, Tull J X and Warren W S 1992 *Phys. Rev. Lett.* **68** 2000–3
[17] Jin L 2019 *Results Phys.* **14** 102508
[18] Lian M, Gu B, Zhang Y, Rui G, He J, Zhan Q and Cui Y 2017 *J. Opt. Soc. Am.* A **34** 2526
[19] Chen W J, Jiang S J, Chen X D, Zhu B, Zhou L, Dong J W and Chan C T 2014 *Nat. Commun.* **5** 5782
[20] Ciattoni A and Palma C 2003 *J. Opt. Soc. Am.* A **20** 2163–71
[21] Zhou M, Chen C, Chen B, Peng X, Peng Y and Deng D 2015 *Chin. Phys.* B **24** 124102
[22] Deng F and Deng D 2016 *Opt. Commun.* **380** 280–6
[23] Zhang J, Zhou K, Liang J, Lai Z, Yang X and Deng D 2018 *Opt. Express* **26** 1290–304
[24] Li D, Peng X, Peng Y, Zhang L and Deng D 2017 *J. Opt. Soc. Am.* B **34** 891–8
[25] Sun C, Lv X, Deng D, Ma B, Liu H and Hong W 2019 *Opt. Commun.* **445** 147–54
[26] Hennani S, Ezzariy L and Belafhal A 2016 *Prog. Electromagn. Res.* M **45** 153–61.
[27] Xu C, Lin L, Huang Z, He D and Deng D 2019 *Chin. Phys.* B **28** 024201
[28] Ciattoni A and Palma C 2004 *Opt. Commun.* **231** 79–92
[29] Xu H F, Huang L M, Sheng Z Q, Tang X and Qu J 2017 *J. Opt.* **19** 085601